Title
Analysis of segmented traveling-wave optical modulators

Journal
Journal of Lightwave Technology, 22(7)

ISSN
0733-8724

Authors
Li, G L
Mason, TGB
Yu, PKL

Publication Date
2004-07-01

Peer reviewed

Analysis of Segmented Traveling-Wave Optical Modulators

G. L. Li, *Member, IEEE*, T. G. B. Mason, *Member, IEEE*, and P. K. L. Yu, *Senior Member, IEEE, Member, OSA*

***Abstract*—A simple and comprehensive modeling approach is developed for analyzing the frequency response of segmented traveling-wave optical modulators. The approach is based on the microwave transmission (ABCD) matrix theory. The case study for a GaAs traveling-wave Mach–Zehnder modulator (MZM) verifies this analysis approach with excellent agreement to the reported experimental results; the analyses for the quantum-well-based MZMs and electroabsorption modulators indicate that the segmented traveling-wave design can provide much better bandwidth than the lumped-element or the continuous-traveling-wave counterparts, with a few decibels penalty in the electrical-to-optical (E/O) conversion gain if low-loss optical waveguides are available. Meandered transmission line design, which provides more design freedom, is also analyzed using this modeling approach.**

***Index Terms*—Electroabsorption (EA), high-speed optical modulation, loaded line, Mach–Zehnder, segmented traveling-wave modulators, slow-wave transmission line, wide bandwidth.**

I. Introduction

EXTERNAL modulation has been shown to have superior performance over direct modulation for wide-bandwidth (> 20 GHz) optical fiber communications [1]. There have been five major types of external optical modulators developed over the past decades for operating at 1.3–1.6 μm laser wavelength range. These include $LiNbO_3$ Mach–Zehnder modulators (MZMs), electroabsorption modulators (EAMs), bulk GaAs MZMs, quantum-well-based InP MZMs and polymer MZMs. Each of these modulator types has its unique pros and cons [2], which makes them suitable for different application needs. To achieve wide bandwidth, most of these modulator types, except EAMs, require traveling-wave electrodes. Even for EAMs, it has been shown that traveling-wave design can provide better performance than the lumped-element counterpart [3]–[6]. The general requirements for traveling-wave electrodes are impedance matching, velocity matching, and low microwave loss.

The traveling-wave designs for different modulator types also have their unique features. For traveling-wave $LiNbO_3$ MZMs, coplanar waveguide (CPW) transmission line is commonly used as the traveling-wave electrode, and ridge optical waveguide together with thick metal (20–30-μm) electrode is required for simultaneous impedance matching and velocity matching [7], [8]. For traveling-wave polymer MZMs, a microstrip transmission lines provide excellent velocity-matching condition since the polymer material has almost the same dielectric constant at the microwave frequencies and at the optical frequencies [9], [10]. For traveling-wave EAMs, low-impedance matching is required, but velocity matching is not so important since the device is usually very short [3]–[6]. One common aspect for the previously mentioned three types of traveling-wave designs is that the modulations in the optical waveguides are continuous, with the optical waveguides being part of the dielectric material of the transmission lines. However, these traveling-wave electrode designs cannot work well for bulk GaAs MZMs and quantum-well-based InP MZMs due to the following reasons. First, to achieve good modulation efficiency, their modulation lengths have to be pretty long compared with microwave wavelengths at high frequencies. This makes the velocity matching very critical, which is unlike the case of traveling-wave EAMs. Second, microwave velocities for transmission lines built on top of GaAs or InP are much faster than the optical group velocities in their optical waveguides, which is opposite to the case of traveling-wave $LiNbO_3$ MZMs. This requires a distinctly different approach for achieving a velocity-matching condition.

To meet the velocity-matching challenge for GaAs MZMs, segmented traveling-wave design has been investigated by many researchers [11]–[18]. The segmented traveling-wave design, as illustrated in Fig. 1, employs a separate transmission line that runs parallel to the optical waveguide, with its microwave velocity faster than the optical group velocity, and its microwave impedance higher than 50 Ω (the impedance of the microwave source). Modulation length (and its capacitance) in the optical waveguide is segmented and periodically connected to the transmission line as capacitive loading, which lowers the microwave velocity and impedance. In the literature, this type of electrode is sometimes called "slow-wave transmission line" or "loaded line." The design goals are to match the lowered microwave velocity with the optical group velocity and match the lowered microwave impedance with 50 Ω. The next section of the paper will show that simultaneous velocity matching and impedance matching can be easily achieved with proper design. Microwave loss can also be very low since the microwave transmission line is separately designed.

This paper provides a simple and comprehensive approach for analyzing the frequency response, as well as other microwave properties, of the segmented traveling-wave optical modulators. In the past, microwave properties of segmented traveling-wave electrodes have been studied experimentally [15], [16], as well as by using some simple inductance–ca-

Manuscript received September 9, 2003; revised December 30, 2003.

G. L. Li is with the Department of Electrical and Computer Engineering, University of California, San Diego, CA 92093-0407 USA and also with Luxtera, Carlsbad, CA 92008-7338 USA (e-mail: guli@ucsd.edu).

T. G. B. Mason is with the Finisar Corporation, Sunnyvale, CA 94089 USA.

P. K. L. Yu is with the Department of Electrical and Computer Engineering, University of California, San Diego, CA 92093-0407 USA (e-mail: yu@ece.ucsd.edu).

Digital Object Identifier 10.1109/JLT.2004.831179

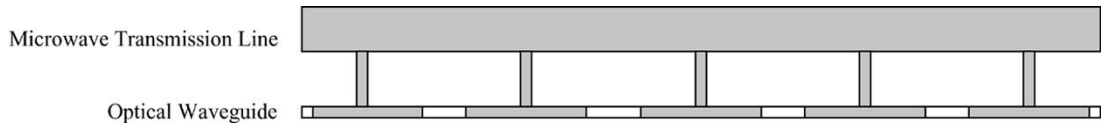

Fig. 1. Schematic diagram to show the traveling-wave electrode design. This can be a phase modulator, an EAM, or one arm of an MZM.

pacitance (*LC*) circuit model [17], [18]. These studies did not involve the analysis of modulation frequency response. An earlier publication [11] showed some calculated frequency responses for segmented traveling-wave GaAs MZMs, but it did not provide a detailed modeling approach and mathematic analysis. In addition, previous research mainly focused on bulk GaAs MZMs. This paper applies the segmented traveling-wave design also for the quantum-well-based InP MZMs and EAMs and analyzes the use of meandered transmission line [19] in these devices. The previously published experimental result of a GaAs MZM will be used to verify this modeling approach.

II. Analytical Approach

First let's use the simple *LC* circuit model to gain some basic understanding of the segmented traveling-wave electrode. The microwave impedance and the microwave velocity index for the unloaded and loaded transmission lines (assumed lossless) can be calculated as

Unloaded line:

$$Z_\mu = \sqrt{\frac{L_\mu}{C_\mu}}, \quad n_\mu = c\sqrt{L_\mu C_\mu} \tag{1}$$

Loaded line:

$$Z_0 = \sqrt{\frac{L_\mu}{C_\mu + C_L}}, \quad n_0 = c\sqrt{L_\mu (C_\mu + C_L)} \tag{2}$$

where L_μ and C_μ are the inductance and capacitance per unit length for the unloaded transmission line, C_L is the loaded capacitance per unit length, and $c \sim 3 \times 10^{11}$ mm/s is the light velocity in vacuum. Z_μ and n_μ are the microwave impedance and phase velocity index values before loading; Z_0 and n_0 are the corresponding parameter values after loading. The traveling-wave design requires matching Z_0 with 50 Ω and matching n_0 with the optical group velocity index (3.4–3.6 for InP and GaAs optical waveguides). From (2), we know that this requires the inductance of the unloaded line to be designed as

$$L_\mu = \frac{n_0 Z_0}{c}. \tag{3}$$

Combining with (1), this is equivalent to the requirement of

$$n_\mu Z_\mu = n_0 Z_0. \tag{4}$$

Equation (2) also indicates that the capacitance of the loaded line should be

$$C_L + C_\mu = \frac{n_0}{cZ_0}. \tag{5}$$

Combining with (1), we can derive

$$C_L = \frac{n_0^2 - n_\mu^2}{cZ_0 n_0}. \tag{6}$$

This analysis indicates that simultaneous impedance matching and velocity matching can be achieved if the unloaded transmission line and the capacitive loading are designed to satisfy the (4) and (6). For loading the same amount of total capacitance, larger C_L is desirable to keep the device shorter, which can reduce the optical loss and enhance the modulation bandwidth. From (6), when n_0 and Z_0 are fixed by the velocity-matching and impedance-matching requirements, n_μ should be as small as possible to improve C_L. This requires the unloaded transmission line to have a fast microwave velocity.

This analysis provides a rough guideline for the segmented traveling-wave electrode design, but it is not sufficient for estimating the modulation frequency response. The frequency response of a segmented traveling-wave modulator is limited not only by the impedance mismatch and the velocity mismatch, but also by the microwave loss, the microwave dispersion and filtering effects due to the periodic capacitive loading, and various parasitic effects. To analyze the frequency response including all these effects, we can use a microwave equivalent circuit model for the segmented traveling-wave electrode, as shown in Fig. 2(a). It represents a total of N segments of active modulation waveguide periodically shunting with a transmission line. Since each active segment is usually very short, it can be modeled by a lumped $L_a R_a C_a$ circuit. The inductance L_a is induced by the connection bridge; the resistance R_a includes the metal bridge resistance and the series resistance of the modulation waveguide; the capacitance C_a is the junction capacitance of the modulation waveguide. It is the voltage across the capacitance C_a that does the actual modulation. A parasitic capacitance shunted with the $L_a R_a C_a$ circuit can also be added if necessary. The microwave transmission line length between any two adjacent bridges is ℓ_0. The microwave source impedance Z_S and the termination impedance Z_T are typically 50 Ω.

To obtain the modulation frequency response, the first step is to calculate the microwave voltages $(V_1, V_2, \ldots V_N)$ across all the loading segments and find the modulation voltages across all the capacitors C_a. Under small-signal modulation, the modulation index for each active segment, no matter what type of optical modulator, is linearly proportional to the modulation voltage across its capacitor C_a. The frequency response of the whole segmented traveling-wave modulator, if all the active segments have the same length, is therefore proportional to the square of the summation of all modulation voltages multiplied by a phase factor caused by the traveling of the modulated optical wave packet.

$V_1, V_2, \ldots V_N$ can be easily calculated using the ABCD transmission matrix method [20]. Note that the transmission matrix for a transmission line with impedance Z_μ, propagation constant $\gamma_\mu = \alpha_\mu + j\beta_\mu$, and length ℓ_0 is

$$T_0 = \begin{bmatrix} \cosh(\gamma_\mu \ell_0) & Z_\mu \sinh(\gamma_\mu \ell_0) \\ Z_\mu^{-1} \sinh(\gamma_\mu \ell_0) & \cosh(\gamma_\mu \ell_0) \end{bmatrix}. \tag{7}$$

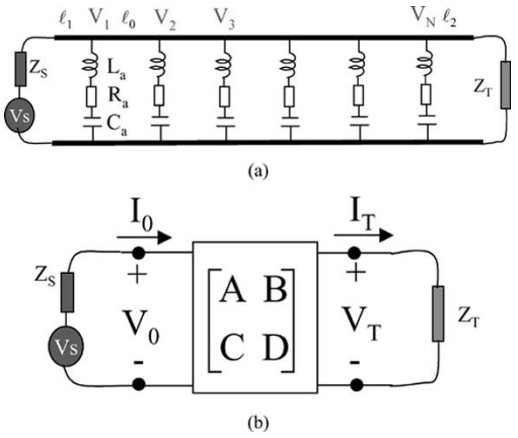

Fig. 2. (a). Microwave equivalent circuit model for segmented traveling-wave optical modulators. (b). Transmission matrix representation of the modulator.

And the transmission matrix for each of the shunted $L_aR_aC_a$ circuit is

$$T_a = \begin{bmatrix} 1 & 0 \\ \left\{R_a + j\left(\omega L_a - \frac{1}{\omega C_a}\right)\right\}^{-1} & 1 \end{bmatrix}. \tag{8}$$

The transmission matrix for the whole traveling-wave electrode can be obtained by multiplying the transmission matrices of all segments, i.e., $T_1(T_aT_0)^{N-1}T_aT_2$, where T_1 and T_2 are the transmission matrices for the transmission lines with length ℓ_1 and ℓ_2, respectively. Assuming the final result takes the form of $\begin{bmatrix} A & B \\ C & D \end{bmatrix}$, as illustrated in Fig. 2(b), the current I_T and the voltage V_T across the termination can be calculated using

$$V_S = V_0 + I_0 Z_S \tag{9}$$

$$\begin{bmatrix} V_0 \\ I_0 \end{bmatrix} = \begin{bmatrix} A & B \\ C & D \end{bmatrix} \times \begin{bmatrix} V_T \\ I_T \end{bmatrix} \tag{10}$$

$$V_T = I_T Z_T. \tag{11}$$

The solution is

$$I_T = \frac{V_S}{AZ_T + B + CZ_SZ_T + DZ_S} \tag{12}$$

$$V_T = \frac{V_SZ_T}{AZ_T + B + CZ_SZ_T + DZ_S}. \tag{13}$$

After I_T and V_T are obtained, $V_N, V_{N-1}, \ldots V_1$ can be calculated iteratively using the transmission matrix method

$$\begin{bmatrix} V_N \\ I_N \end{bmatrix} = T_2 \begin{bmatrix} V_T \\ I_T \end{bmatrix}, \begin{bmatrix} V_{N-1} \\ I_{N-1} \end{bmatrix} = T_0T_a \begin{bmatrix} V_N \\ I_N \end{bmatrix}, \cdots \begin{bmatrix} V_1 \\ I_1 \end{bmatrix} = T_0T_a \begin{bmatrix} V_2 \\ I_2 \end{bmatrix}. \tag{14}$$

The modulation voltage across the nth capacitor C_a ($n = 1, \ldots N$) is just V_n multiplied by a factor of $(1 - \omega^2 L_aC_a + j\omega R_aC_a)^{-1}$. The microwave phase factor at the nth segment due to the traveling time of the modulated optical wave packet is $\exp[j\omega(\ell_1 + (n-1)\ell_0)/v_o]$, where v_o is the optical group velocity in the optical waveguide. In order to normalize the frequency response, we consider the ideal case when all the modulation voltages are equal to the input microwave voltage $V_S/2$. Taking $NV_S/2$ as the normalization constant for the summation of the voltage, the normalized frequency response of the segmented traveling-wave optical modulators can be expressed as

$$M(f) = \left| \frac{2}{NV_S} \sum_{n=1}^{\mathrm{N}} V_n e^{j\omega\{\ell_1 + (n-1)\ell_0\}/v_o} \frac{1}{1 - \omega^2 L_aC_a + j\omega R_aC_a} \right|^2. \tag{15}$$

This modeling of the modulator frequency response is simple and straightforward, and it has included most of the nonideal microwave effects, although maybe implicitly. During the course of calculating V_n, the impedance mismatch takes effect through (9)–(11); microwave loss is considered through the parameters α_μ and R_a; microwave filtering and dispersion effects due to the periodic loading are reflected in the multiplication of transmission matrices $T_1(T_aT_0)^{N-1}T_aT_2$. The velocity mismatch is included by taking into account the microwave phase factor due to the traveling time of the modulated optical wave. The $L_aR_aC_a$ circuit model reflects some parasitic effects. To use this modeling approach, we need to know the microwave properties of the unloaded transmission line, which can be easily calculated since it is usually a standard design; we also need to have the parameter values of $L_aR_aC_a$, which can be obtained either by empirical estimation or by experiments.

For the loaded transmission line, the ABCD coefficients of the resulting transmission matrix can be used to calculate its microwave properties. Its impedance is just $(B/C)^{1/2}$, as implied by (7); its propagation constant is $a\cosh(A)/[\ell_1 + (N-1)\ell_0 + \ell_2]$, from which the microwave loss and the microwave phase velocity of the loaded line can be obtained. The loaded line appears to be dispersive, as its microwave impedance and phase velocity are frequency dependent.

III. Segmented Traveling-Wave GaAs MZM

Segmented traveling-wave GaAs MZMs have been investigated for more than a decade. Their performance is now approaching that of $LiNbO_3$ MZMs. Two major types of segmented traveling-wave electrodes have been developed for GaAs MZMs: one uses a coplanar-strip (CPS) transmission line, with a doped AlGaAs layer at the bottom of the two optical waveguides to implement series push–pull [11]–[13]; the other uses a CPW transmission line with all layers undoped to implement parallel push–pull [14], [15]. The series push–pull version has achieved 50-GHz bandwidth with 12.9 V of V_π at 1530-nm wavelength [12] and 33-GHz bandwidth with 4.7 V of V_π at similar optical wavelength [13]; the parallel push–pull version has achieved $>$ 50-GHz bandwidth with 16.8 V of V_π at 1550-nm wavelength [14]. The performance in [13] is suitable for 40-Gb/s modulation. Its device structure and measured frequency response are used here for verifying our modeling approach.

According to [13], the electrode was 16 mm long. Microwave source impedance Z_S was 50 Ω. Since the CPS transmission line was built on top of a GaAs substrate, its microwave phase velocity index n_μ was approximately $[(1 + \varepsilon_{\mathrm{GaAs}})/2]^{1/2} \sim 2.65$,

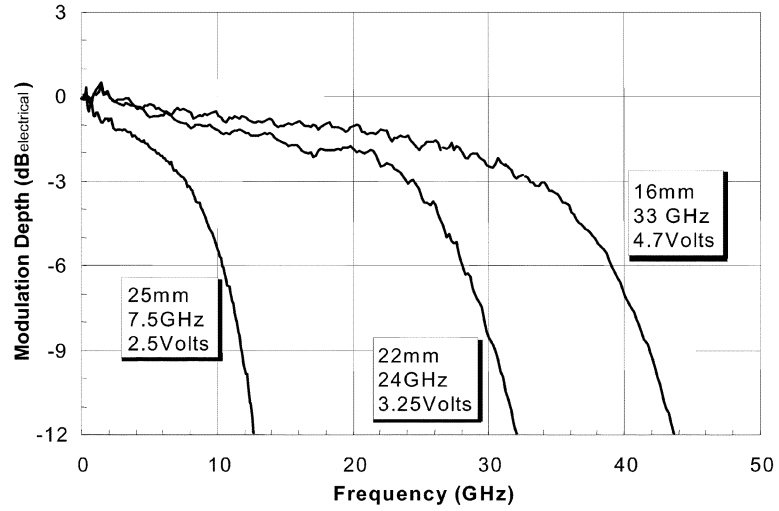

(a)

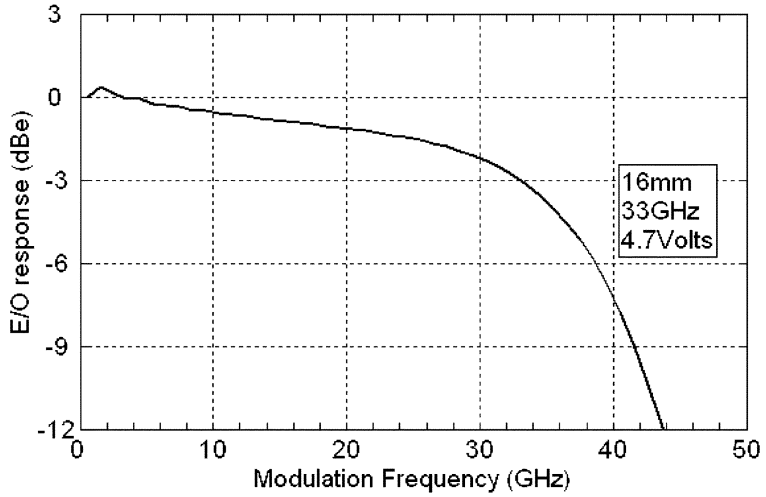

(b)

Fig. 3. Comparison between (a) the measured frequency response (the curve with 16 mm length) (*courtesy of* [13]) and (b) the calculated frequency response using our modeling approach.

where $\varepsilon_{\mathrm{GaAs}} \sim 13$ is the dielectric constant of GaAs. For the GaAs optical waveguide, the optical group velocity index n_o is ~ 3.6. If the loaded-line impedance was targeted at $Z_0 = 50\ \Omega$, we can derive $Z_\mu = 68\ \Omega$ for the unloaded line using (4). The microwave loss coefficient α_μ for the unloaded line was around 0.006 $\mathrm{f}^{1/2}$ mm^{-1} (frequency in gigahertz), i.e., 3.3 dB/cm @40 GHz. We assume the device used 50 active segments, with a 70% fill factor [12]. Therefore, L_0 was 320 μm long, and the active length for each segment was 224 μm. Based on their device structure, the parameter values of L_a, C_a, and R_a (note they represent two segments in the series connection) are empirically estimated as $L_a \sim 100$ pH, $R_a \sim 4\ \Omega$, and $C_a \sim 35$ fF. The Z_T value is set at 42 Ω. Most of these assumed or estimated parameter values have been slightly adjusted during the calculation in order to produce a close fit for the measured frequency response.

The measured frequency response curves are shown in Fig. 3(a), while the calculated curve is presented in Fig. 3(b). The calculated curve for the device with 16-mm-long electrode matches closely with the corresponding measured curve. The small bump at low frequency (1–2 GHz) is due to microwave resonance caused by the 42-Ω termination. Although some of the parameters used in this calculation were based on reasonable estimations and may not exactly represent the actual device, the capability of generating frequency response matching closely with the experiment shows that our modeling approach is valid and that it can explain the behavior of the measured frequency response.

Our modeling tool can further be used to optimize the device design. For instance, if the total active length (11.2 mm) of the previously described device is divided into a different number of segments, its frequency response can be very different. Fig. 4 shows the calculated frequency response curves for the device using 25, 50, 100, and 200 segments. During the calculation, the C_a and R_a values have been scaled with the active length for each segment, and the bridge inductance L_a is fixed at 100 pH.

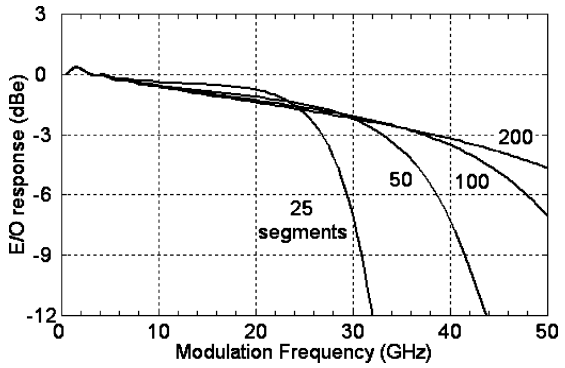

Fig. 4. Calculated frequency responses for the GaAs MZM using different numbers of segments.

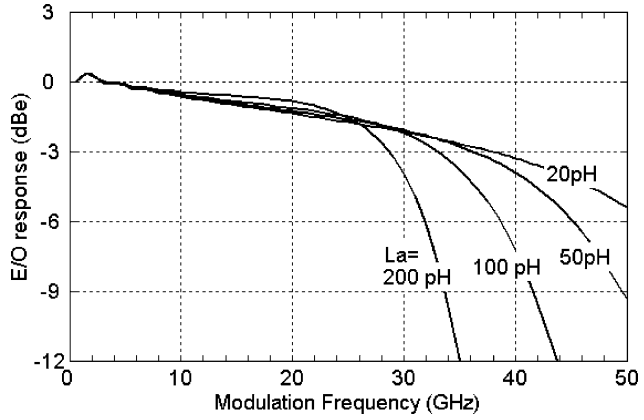

Fig. 5. Calculated frequency responses for the GaAs MZM with different bridge inductances.

In this example, finer segmentation leads to better 3-dB bandwidth, as shown in Fig. 4. This is not always the case, however, for all devices. Coarse segmentation sometimes can cause a small hump in the frequency response curve, which may improve the 3-dB bandwidth. Nevertheless, finer segmentation reduces the dispersion effect and increases the cutoff frequency for the loaded line. This generally results in better modulation response at high frequency, even though it may not lead to a better 3-dB bandwidth.

Another parameter for optimization is the bridge inductance L_a. Fig. 5 shows the calculated frequency response curves using different L_a values, with all other parameters kept the same. We can see that the effect of different inductance values is very similar to the effect of different segmentations, with smaller inductance corresponding to finer segmentation. In practice, the L_a value can be controlled by adjusting the bridge length, width, and thickness.

Since the loaded line is dispersive, the capacitive loading can be so designed that the best velocity matching and impedance matching are achieved at high frequency. This implies an intentional velocity mismatch and impedance mismatch at low frequency by using underfill [12]. It may flatten the frequency response curve within the 3-dB-bandwidth range. The calculated dispersion of the loaded line for the GaAs MZM in this example is shown in Fig. 6.

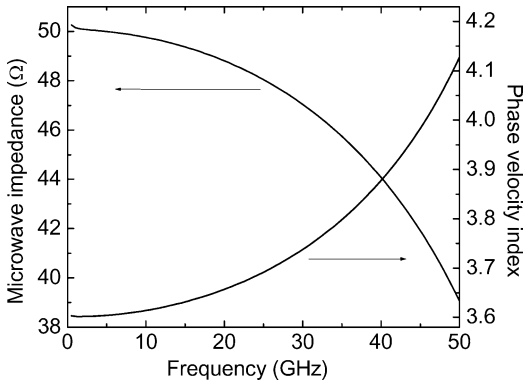

Fig. 6. Calculated microwave dispersion for the loaded line of the GaAs MZM.

IV. Segmented Traveling-Wave Quantum-Well-Based MZM

Quantum wells using InP alloy materials can have a large voltage-controlled index change at 1.3–1.6-μm wavelength range. This index change is induced by the quantum-confined Stark effect (QCSE), which increases very fast with the increased electric field. Therefore, it requires a thin active layer to provide a large electrical field, and the series push–pull may not be an efficient way because it halves the electric field in each optical waveguide. Most of the reported quantum-well-based MZM used lumped-element electrodes and single-arm modulation [21]–[24]. In these previous works, the active modulation layer typically consisted of 20–30 quantum wells, with a total intrinsic layer thickness of $\sim$ 0.4 μm. The MQW detuning energy was set around 60 meV to keep optical absorption loss low. With 600-μm-long active length, this configuration was able to achieve a V_π around 4–5 V, and the best bandwidth achieved was 15 GHz [21].

Segmented traveling-wave electrode design can be considered for improving the device bandwidth. For a waveguide with 0.4-μm intrinsic layer thickness and 2-μm width, the capacitance is typically 0.6–0.8 pF/mm. The total capacitance of a 600-μm-long waveguide is 0.4–0.5 pF. If we use a transmission line built on top of InP to load this capacitance ($C_L \sim 0.9$ pF/cm), it will require an $\sim$ 5-mm-long electrode, and the optical waveguide will be too long and too lossy. On the other hand, if we build a transmission line with faster microwave phase velocity, for example, a microstrip line with low-k dielectric material [19], the loading capacitance C_L can be improved by a factor of two, and the electrode length can be halved.

The first step in the design is to assure the impedance matching using (4). The fast microstrip line typically has a velocity index of $n_\mu \sim 1.4$, and the InP optical waveguide has a group velocity index of $n_0 \sim 3.4$. If the loaded line has to match with impedance $Z_0 = 50\ \Omega$, it will require $Z_\mu \sim 121\ \Omega$. In practice, it is difficult to achieve this high impedance together with low microwave loss for a microstrip transmission line. It will require a pretty thick dielectric layer that is very difficult to fabricate. Practically, achievable high impedance is $\sim 80\ \Omega$. To match impedance using this practical microstrip line, one has to either lower the target impedance Z_0 to $\sim$ 33 Ω or use a meandered microstrip line to match with a Z_0 of 50 Ω [19].

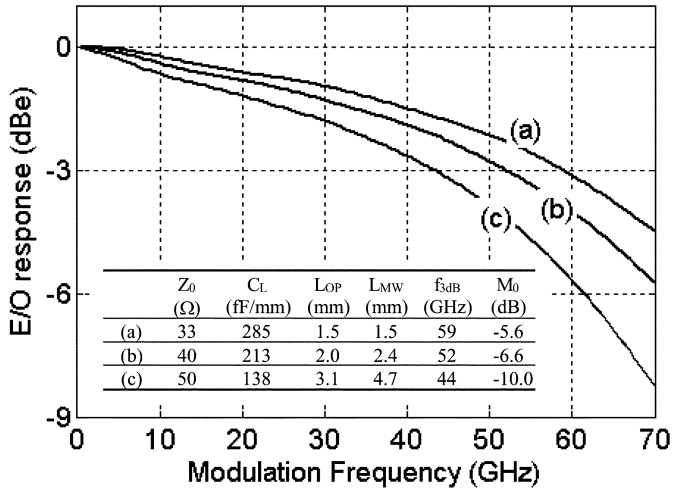

	Z_0 (Ω)	C_L (fF/mm)	L_{OP} (mm)	L_{MW} (mm)	f_{3dB} (GHz)	M_0 (dB)
(a)	33	285	1.5	1.5	59	-5.6
(b)	40	213	2.0	2.4	52	-6.6
(c)	50	138	3.1	4.7	44	-10.0

Fig. 7. Calculated frequency responses for quantum-well-based segmented traveling-wave MZMs using different terminator impedance Z_0. The inset table shows the termination impedance Z_0, the capacitance loading capability C_L (the unit is femto Farade per millimeter of optical waveguide), the optical waveguide length $L_{\rm OP}$, the microstrip line length $L_{\rm MW}$, the resulting 3-dB bandwidth $\rm f_{3\,dB}$, and the relative E/O conversion gain M_0 (at 0 Hz) compared with the 0.6-mm-long lumped element design using 50-Ω matching resistance.

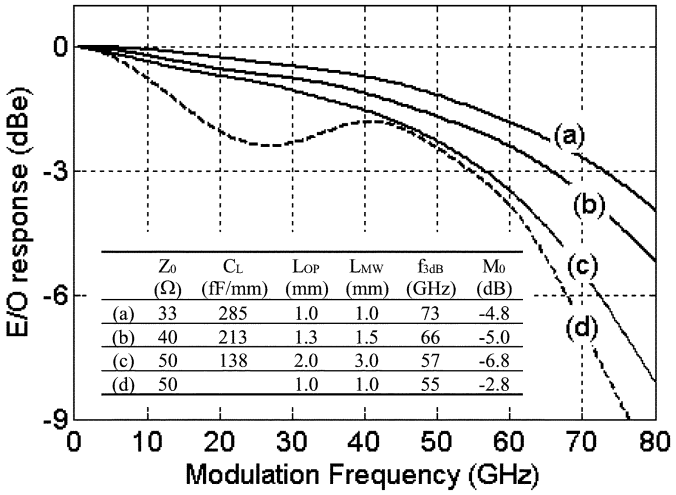

	Z_0 (Ω)	C_L (fF/mm)	L_{OP} (mm)	L_{MW} (mm)	f_{3dB} (GHz)	M_0 (dB)
(a)	33	285	1.0	1.0	73	-4.8
(b)	40	213	1.3	1.5	66	-5.0
(c)	50	138	2.0	3.0	57	-6.8
(d)	50		1.0	1.0	55	-2.8

Fig. 8. Calculated frequency responses for segmented traveling-wave EAMs using different terminator impedance Z_0. The inset table shows the terminator impedance Z_0, the capacitance loading capability C_L (the unit is femto Farade per millimeter of optical waveguide), the optical waveguide length $L_{\rm OP}$, the microstrip line length $L_{\rm MW}$, the resulting 3-dB bandwidth $\rm f_{3dB}$, and the relative E/O conversion gain M_0 (at 0 Hz) compared with the 0.3-mm-long lumped-element design using 50-Ω matching resistance.

The latter approach is equivalent to making the microwave travel slower so that the n_μ value is higher. For example, if the microstrip line is meandered so that its length is 1.5 times of the optical waveguide length, the effective microwave velocity will be 1.5 times slower, and the effective n_μ will be increased to ~ 2.1. In this case, impedance matching with $Z_0 = 50\ \Omega$ can be satisfied. After the values of Z_0, Z_μ, n_0, and n_μ (effective) are determined from the impedance-matching condition, the capacitance loading capability C_L can be calculated using (6) and then the optical waveguide length and the transmission line length can be determined. Note that the higher effective n_μ resulted from the meandered transmission line approach reduces C_L, thus making the device longer.

To quantitatively evaluate the frequency response and the advantage of the segmented traveling-wave design for the quantum-well-based MZMs, our numerical modeling tool can be used. During the simulation, the total modulation length is fixed at 600 μm, which is the same as the lumped-element design, but it is now divided into ten segments and periodically loaded to a microstrip line with an impedance of 80 Ω and a phase velocity index of 1.4. The optical waveguide length ($L_{\rm OP}$) and the transmission line length ($L_{\rm MW}$) are determined for different matching impedances Z_0 (33, 40, and 50 Ω) using the approach described in the last paragraph. Microwave loss for the unloaded line is assumed to be $0.01\rm f^{1/2}\ mm^{-1}$ (f is the frequency in gigahertz unit), i.e., 0.55 dB/mm @40 GHz. For each 60-μm-long active segment, it is reasonable to take $C_a \sim 43$ fF, $R_a \sim 15\ \Omega$, and $L_a \sim 30$ pH. The calculated frequency response curves are presented in Fig. 7, with an inset table showing the corresponding design parameters. The microwave source impedance is assumed as 50 Ω in all cases. Fig. 7 shows that with the loaded transmission line designed to match with the termination impedance Z_0 of 33, 40, and 50 Ω, the segmented traveling-wave MZMs will have bandwidths of 59, 52, and 44 GHz, respectively. As a comparison, the 600-μm-long lumped-element MZMs using these termination impedances can only have bandwidths of 18, 16, and 14 GHz, respectively. The dc V_π of the segmented traveling-wave MZMs should be the same as that of the lumped-element MZMs, since their total modulation lengths are the same.

The penalty for the segmented traveling-wave design is some extra optical loss due to the passive optical waveguide. The inset table in Fig. 7 lists the relative E/O conversion gain $\rm M_0$ (at 0 Hz) compared with the 600 μm long lumped element MZM using 50 Ω matching resistance. The negative values of $\rm M_0$ come from two sources. One source is the extra optical loss due to the passive optical waveguide. Assuming that the optical loss in the passive optical waveguide is 2 dB/mm, this source lowers $\rm M_0$ by 3.6 dB, 5.6 dB and 10.0 dB for the designs (a), (b) and (c), respectively. The other source is due to the termination impedance less than 50 Ω. This source lowers $\rm M_0$ by 2.0 dB, 1.0 dB and 0 dB for designs (a), (b) and (c), respectively. Fig. 7 indicates that design (a), which uses 33 Ω terminator impedance and straight transmission line, has the best gain-bandwidth product and the shortest device length (1.5 mm). However, if the system requires higher termination impedance for controlling microwave return loss, designs (b) and (c) will have to be used, in which meandered transmission line helps to achieve good impedance matching condition.

V. Segmented Traveling-Wave EAM

Among all the five major types of optical modulators, the EAM is the smallest device, and it is the most compatible with monolithic integration with other optoelectronic components. Due to their high modulation efficiency, EAMs are usually very short. For 10-Gb/s digital modulation, the EAM can be 200–300 μm long; for 40-Gb/s modulation, the EAM active waveguide length is typically around 100 μm. These EAMs can provide a 15–20-dB extinction ratio per 100-μm modulation length with less than 3-V voltage swing, and they only require

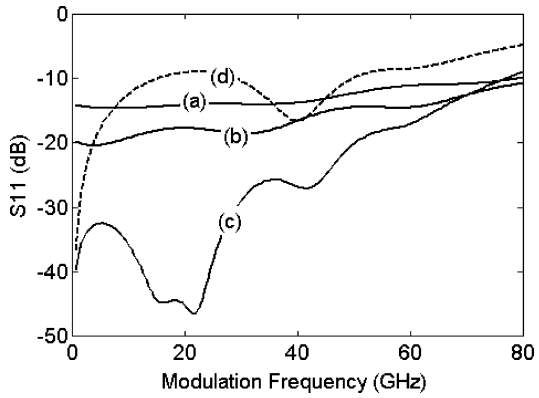

Fig. 9. Microwave return loss from the segmented traveling-wave EAMs to the 50-Ω source. The curve labels (a), (b), (c), and (d) correspond to the curve labels in Fig. 8.

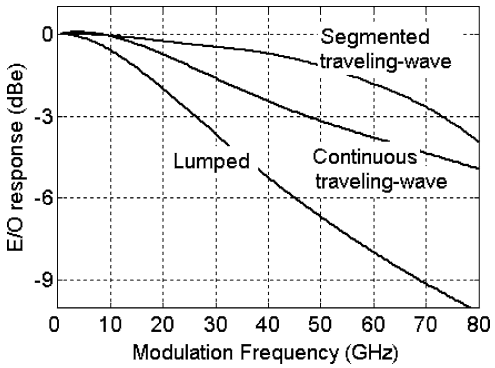

Fig. 10. Calculated frequency responses for the EAMs using segmented traveling-wave design (1 mm long) with 33-Ω termination, continuous traveling-wave design (0.3 mm long) with 25-Ω termination, and lumped-element design (0.3 mm long) with 33-Ω termination.

simple lumped-element electrodes to achieve their target bandwidths. However, for analog applications, wider bandwidth and higher modulation efficiency may be required. In this case, the traveling-wave electrode can be used to improve the performance [3]–[6], [19]. The microwave transmission lines for most of the previously demonstrated traveling-wave EAMs (TWEAM) were built directly on top of the optical waveguides, and they generally had a low microwave impedance (20–30 Ω), slow microwave velocity, and large microwave loss. Fortunately, these devices were all short in length (200–300 μm) so that the velocity mismatch and microwave loss were not severe problems. With low-impedance termination, a bandwidth as high as 67 GHz had been achieved for a 250-μm-long device [5]. The penalty of the low-impedance termination for TWEAMs is that some modulation efficiency is sacrificed. For example, by using 11-Ω termination in [5], 8.8-dB RF gain is sacrificed at low frequency compared with the usual 50-Ω termination.

With the segmented traveling-wave design for EAMs [19], it is possible to achieve better performance. In the exemplary designs, we assume the total active modulation length is 300 μm. It is divided into six segments and loaded to a microstrip transmission line same as the one in the last section. For each 50-μm -long active segment, we take $C_a \sim 45$ fF, $R_a \sim 16\ \Omega$, and $L_a \sim 30$ pH. The design considerations for impedance matching are exactly the same as in the last section. The frequency response curves calculated using our numerical modeling tool are presented in Fig. 8. The curves (a), (b), and (c) with loaded-line impedance matched to the termination impedance of 33, 40, and 50 Ω show bandwidths of 73, 66, and 57 GHz, respectively. The efficiency compromise M_0 for the three designs is 4.8–6.8 dB, which is several decibels better than the continuous TWEAM with a similar bandwidth [5]. The corresponding microwave reflections to the 50-Ω source from these segmented traveling-wave EAMs (STEAM) are shown in Fig. 9.

With our modeling tool, more flexible designs can be evaluated. For example, one can modify the above design (a) by changing the termination impedance from 33 Ω to 50 Ω. This leads to 2 dB better E/O conversion gain M_0. Its frequency response is shown as curve (d) in Fig. 8. A larger bridge inductance ($L_a = 80$ pH) is used in this case to lift up the frequency response in the 20–60 GHz range. The resulted bandwidth is 55 GHz, close to the bandwidth of design (c), but with 4 dB better gain. Consequently, design (d) has larger gain-bandwidth product than designs (a), (b) and (c). The penalty of design (d) is that it has the worst microwave reflection to the 50 Ω source, as shown in Fig. 9.

Using the same waveguide design and 300-μm total modulation length, we have also calculated the frequency responses for the lumped-element EAM and the continuous TWEAM, and the results are plotted in Fig. 10, together with the frequency response of the 1-mm-long STEAM terminated by 33 Ω. Only 26-GHz bandwidth can be achieved when using lumped-element electrode terminated with 33 Ω resistor, which is much less than the 73 GHz bandwidth of the STEAM. The continuous TWEAM requires lower impedance termination in order to achieve wide bandwidth. When 25-Ω termination is used, the calculated frequency response based on the approach from [3] shows a 3-dB bandwidth of 47 GHz, which is 26 GHz lower than the bandwidth of the STEAM. During the calculation for TWEAM, we assumed its transmission line inductance $L_m = 0.4$ nH/mm and conduction resistance $R_{\mathrm{con}} = 5\ \Omega\text{-}\ \mathrm{mm}^{-1}\text{-}\ \mathrm{GHz}^{-1/2}$ [3].

VI. Conclusion

This paper described the development of a simple and comprehensive modeling approach for analyzing the frequency response, as well as other microwave properties, for segmented traveling-wave optical modulators. This approach is based on the microwave transmission (ABCD) matrix theory and can be implemented by a simple computer program. It can be used as an optimization tool for the segmented traveling-wave modulator design. We have applied this modeling tool for analyzing a segmented traveling-wave GaAs MZM and obtained a frequency response curve that is very close to the measured curve from the publication. This verifies our analysis approach.

This modeling tool was also further used to design segmented traveling-wave quantum-well-based MZMs and EAMs using InP and its alloy materials. For the InP MZM with a DC V_π target of 4–5 V under single-arm modulation, 44–59-GHz bandwidth can be achieved by using segmented traveling-wave design, whereas lumped-element design can only achieve less than

20 GHz. For EAMs with 300-μm total modulation length, segmented traveling-wave design provides 57–73-GHz bandwidth, which is more than a 20-GHz improvement compared with the continuous TWEAM and $\sim$ 40-GHz improvement compared with the lumped-element EAM. The only disadvantage for the segmented traveling-wave MZMs and EAMs is some extra optical loss due to the passive optical waveguide.

The paper also showed that the proposed simple modeling tool can be used to optimize the device design. The segmentation effect, the inductance effect, and the microwave loss effect can be conveniently evaluated using this tool. The meandered transmission line design, which in some cases can help to achieve better impedance matching and velocity matching, can also been analyzed using this tool. These analyses have demonstrated that the proposed modeling tool is very useful to the design of various types of segmented traveling-wave optical modulators.

ACKNOWLEDGMENT

G. L. Li and P. K. L. Yu would like to acknowledge the sponsorship of the National Science Foundation—Advanced Networking Infrastructure and Research Program (NSF-ANIR), Air Force Research Laboratories, Rome, Italy, and the Defense Advanced Research Projects Agency (DARPA) for the optical modulator research at the University of California at San Diego.

REFERENCES

[1] C. H. Cox III, G. E. Betts, and L. M. Johnson, "An analytic and experimental comparison of direct and external modulation in analog fiber-optic links," *IEEE Trans. Microwave Theory Tech.*, vol. 38, pp. 501–509, May 1990.

[2] G. L. Li and P. K. L. Yu, "Optical intensity modulators for digital and analog applications," *J. Lightwave Technol.*, vol. 21, pp. 2010–2030, Sept. 2003.

[3] G. L. Li, C. K. Sun, S. A. Pappert, W. X. Chen, and P. K. L. Yu, "Ultra high-speed traveling wave electroabsorption modulator: Design and analysis," *IEEE Trans. Microwave Theory Tech.*, vol. 47, pp. 1177–1783, July 1999.

[4] Y. -J. Chiu, H. -F. Chou, V. Kaman, P. Abraham, and J. E. Bowers, "High extinction ratio and saturation power traveling-wave electroabsorption modulator," *IEEE Photon. Technol. Lett.*, vol. 14, pp. 792–794, June 2002.

[5] S. Irmscher, R. Lewen, and U. Eriksson, "InP–InGaAsP high-speed traveling-wave electroabsorption modulators with integrated termination resistors," *IEEE Photon. Technol. Lett.*, vol. 14, pp. 923–925, July 2002.

[6] G. L. Li, S. A. Pappert, P. Mages, C. K. Sun, W. S. C. Chang, and P. K. L. Yu, "High-saturation high-speed traveling-wave InGaAsP–InP electroabsorption modulator," *IEEE Photon. Technol. Lett.*, vol. 13, pp. 1076–1078, Oct. 2001.

[7] K. Noguchi, O. Mitomi, and H. Miyazawa, "Millimeter-wave Ti:$LiNbO_3$ optical modulators," *J. Lightwave Technol.*, vol. 16, pp. 615–619, Apr. 1998.

[8] W. K. Burns, M. M. Howerton, R. P. Moeller, R. W. McElhanon, and A. S. Greenblatt, "Low drive voltage, 40 GHz $LiNbO_3$ modulators," in *Optical Fiber Communication 1999 (OFC'99) Tech. Dig.*, 1999, ThT1–1, pp. 284–286.

[9] C. C. Teng, "Traveling-wave polymeric optical intensity modulator with more than 40 GHz of 3 dB electrical bandwidth," *Appl. Phys. Lett.*, vol. 60, pp. 1538–1540, 1992.

[10] W. Wang, Y. Shi, D. J. Olson, W. Lin, and J. H. Bechtel, "Push–pull poled polymer Mach–Zehnder modulators with a single microstrip line electrode," *IEEE Photon. Technol. Lett.*, vol. 11, pp. 51–53, Jan. 1999.

[11] R. G. Walker, "High-speed III–V semiconductor intensity modulators," *IEEE J. Quantum Electron.*, vol. 27, pp. 654–667, Mar. 1991.

[12] ——, "Electro-optic modulation at mm-wave frequencies in GaAs/AlGaAs guided wave devices," in *IEEE LEOS Annu. Meeting (LEOS'95)*, San Francisco, CA, Oct. 1995, pp. 118–119.

[13] R. G. Walker, R. A. Griffin, R. D. Harris, R. I. Johnstone, N. M. B. Perney, and N. D. Whitbread, "Integrated high-functionality GaAs modulators for 10 & 40 Gb/s transmission," in *Proc. Integrated Photonics Research 2001 (IPR'2001)*, Monterey, CA, 2001, IME3.

[14] R. Spickermann, S. R. Sakamoto, M. G. Peters, and N. Dagli, "GaAs/AlGaAs traveling wave electro-optic modulator with an electric bandwidth $>$ 40 GHz," *Electron. Lett.*, vol. 32, pp. 1095–1096, 1996.

[15] S. R. Sakamoto, R. Spickermann, and N. Dagli, "Narrow gap coplanar slow wave electrode for travelling wave electro-optic modulators," *Electron. Lett.*, vol. 31, pp. 1183–1185, 1995.

[16] N. A. F. Jaeger, F. Rahmatian, H. Kato, R. James, E. Berolo, and Z. K. F. Lee, "Velocity-matched electrodes for compound semiconductor traveling-wave electrooptic modulators: Experimental results," *IEEE Microwave Guided Wave Lett.*, vol. 6, pp. 82–84, Feb. 1996.

[17] N. A. F. Jager and Z. K. F. Lee, "Slow-wave electrode for use in compound semiconductor electrooptic modulators," *IEEE J. Quantum Electron.*, vol. 28, pp. 1778–1784, Aug. 1992.

[18] C. L. Goldsmith and R. Magnusson, "Bandwidth improvements for loaded-line traveling wave electro-optic modulators," in *IEEE MTT-S Dig., Int. Microwave Symp.*, May 1995, pp. 1499–1502.

[19] R. Lewen, S. Irmscher, U. Westergren, L. Thylen, and U. Eriksson, "Ultra high-speed segmented traveling-wave electroabsorption modulators," in *Optical Fiber Communication (OFC'03) Tech. Dig.*, 2003, PD38.

[20] D. M. Pozar, *Microwave Engineering*. Reading, MA: Addison-Wesley, 1990.

[21] C. Rolland, R. S. Moore, F. Shepherd, and G. Hillier, "10 Gbit/s, 1.56 mm multiple quantum well InP/InGaAsP Mach–Zehnder optical modulator," *Electron. Lett.*, vol. 29, pp. 471–472, 1993.

[22] K. Wakita, O. Mitomi, I. Kotaka, S. Nojima, and Y. Kawamura, "High-speed electrooptic phase modulators using InGaAs/InAlAs multiple quantum well waveguides," *IEEE Photon. Technol. Lett.*, vol. 1, pp. 441–442, Dec. 1989.

[23] D. Penninckx and P. Delansay, "Comparison of the propagation performance over standard dispersive fiber between InP-based π-phase-shifted and symmetrical Mach–Zehnder modulators," *IEEE Photon. Technol. Lett.*, vol. 9, pp. 1250–1252, Sept. 1997.

[24] J. Yu, C. Rolland, D. Yevick, A. Somani, and S. Bradshaw, "A novel method for improving the performance of InP/InGaAsP multiple-quantum-well Mach–Zehnder modulators by phase shift engineering," in *Proc. Integrated Photonics Research 1996 (IPR'96)*, 1996, 1TuG4, pp. 376–379.

G. L. Li (S'97–A'01–M'01) received the Ph.D. degree in electrical engineering from the University of California, San Diego (UCSD), in 2002.

From 2001 to 2002, he worked at Lucent Technologies/Agere Systems as a Principal Device Designer for the development of several high-speed optoelectronics components. In 2003, he joined UCSD as a Researcher, while working as a Technical Consultant for Vitesse. At the end of 2003, he joined Luxtera, working as a lead designer for developing high-speed optoelectronic devices on Si substrate. His research interests include advanced semiconductor photonic devices and their integration with electronic circuits.

T. G. B. Mason (M'03), photograph and biography not available at the time of publication.

P. K. L. Yu (SM'91) received the Ph.D. degree in applied physics at the California Institute of Technology (Caltech), Pasadena, in 1983.

In September 1983, he became a Faculty Member in the Department of Electrical and Computer Engineering at the University of California at San Diego (UCSD), where he has been a Professor since 1993. At UCSD, he conducts research in materials and devices for fiber-optic and optoelectronics applications, particularly for microwave transmission over fiber. His group has developed high-power optical detectors and high-linearity waveguide modulators.

Dr. Yu is a Member of the Optical Society of America (OSA).